Conformal Structures and Period Matrices of Polyhedral Surfaces

Alexander Bobenko* Christian Mercat† Markus Schmies*

March 7, 2008

Abstract

We recall the theory of linear discrete Riemann surfaces and show how to use it in order to interpret a surface embedded in $\mathbb{R}^3$ as a discrete Riemann surface and compute its basis of holomorphic forms on it. We present numerical examples, recovering known results to test the numerics and giving the yet unknown period matrix of the Lawson genus-2 surface.

1 Introduction

Finding a conformal parameterization for a surface and computing its period matrix is useful in a lot of contexts, from statistical mechanics to computer graphics.

The 2D-Ising model [18, 8, 9] for example takes place on a cellular decomposition of a surface whose edges are decorated by interaction constants, understood as a discrete conformal structure. In certain configurations, called critical temperature, the model exhibits conformal invariance properties in the thermodynamical limit and certain statistical expectations become discrete holomorphic at the finite level. The computation of the period matrix of higher genus surfaces built from the rectangular and triangular lattices from discrete Riemann theory has been addressed in the cited papers by Costa-Santos and McCoy.

Global conformal parameterization of a surface is important in computer graphics [16, 12, 2, 25, 17, 26] in issues such as texture mapping of a flat picture onto a curved surface in $\mathbb{R}^3$. When the texture is recognized by the user as a natural texture known as featuring round grains, these features should be preserved when mapped on the surface, mainly because any shear of circles into ellipses is going to be wrongly interpreted as suggesting depth increase. Characterizing a surface by a few numbers is as well a desired feature in computer graphics, for

*Technische Universität Berlin, FZT 86, F5, FB 3 Mathematik, MA 3-2 Straße des 17. Juni 136 10623 Berlin, Germany `bobenko, schmies@math.tu-berlin.de`

†I3M, Université Montpellier 2 c.c. 51 F-34095 Montpellier cedex 5 France `mercat@math.univ-montp2.fr`

problems like pattern recognition. Computing numerically the period matrix of a surface has been addressed in the cited papers by Gu and Yau.

This paper recalls the general framework of discrete Riemann surfaces theory [14, 13, 18, 4] and the computation of period matrices within this framework (based on theorems and not only numerical analogies). We describe the straightforward translations of these theorems into algorithms, their implementation and discuss some tests performed to check the validity of the approach.

We chose first surfaces with known period matrices at different level of refinement, namely some genus two surfaces made out of squares and the Wente torus, then computed the yet unknown period matrix of the Lawson surface, recognized it numerically as one of the tested surfaces, which allowed us to conjecture their conformal equivalence, and finally prove this equivalence.

2 Discrete conformal structure

Consider a polyhedral surface in $\mathbb{R}^3$. It has a unique Delaunay tesselation, generically a triangulation [5]. That is to say each face is associated with a circumcircle drawn on the surface and this disk contains no other vertices than the ones on its boundary. Let's call Γ the graph of this cellular decomposition. Each edge $(x, x') = e \in \Gamma_1$ is adjacent to a pair of triangles, associated with two circumcenters y, y'. The ratio of the (intrinsic) distances between the circumcenters and the length of the (orthogonal) edge e is called $\rho(e)$.

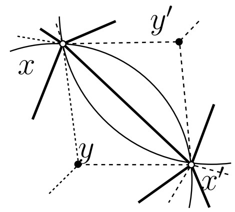

$$\rho = \frac{|y' - y|}{|x' - x|}$$

We call this data of a graph Γ, whose edges are equipped with a positive real number a *discrete conformal structure*. Two surfaces with the same discrete conformal structure belong to the same conformal equivalence class. Among them, the flat one are particularly interesting since the plane can be identified with the field of complex numbers. It leads to a theory of discrete Riemann surfaces and discrete analytic functions that shares a lot of features with the continuous theory [14, 13, 18, 19, 20, 4, 11]. We are going to summarize these results.

In our examples, the triangulations are indeed Delaunay. For theoretical reasons, we have chosen the **intrinsic** flat metric with conic singularities given by the triangulation. It does not depend on the immersion of the surface whereas the Euclidean distance in $\mathbb{R}^3$, called the **extrinsinc** distance, is easier to compute and depends on the immersion. For a surface which is refined and flat enough, the difference is not large. We compared numerically the two ways to compute ρ. The conclusion is that, in the examples we tested, the intrinsic distance is marginally better, see Sec. 4.2.

The circumcenters and their adjacencies define a 3-valent abstract (locally planar) graph, dual to the graph of the surface, that we call Γ^*. We equip the dual edge $(y, y') = e^* \in \Gamma_1^*$ of the positive real constant $\rho(e^*) = 1/\rho(e)$. We define $\Lambda := \Gamma \oplus \Gamma^*$ the *double* graph. Each pair of dual edges $e, e^* \in \Lambda_1$, $e = (x, x') \in \Gamma_1$, $e^* = (y, y') \in \Gamma_1^*$, are seen as the diagonals of a quadrilateral, composing the faces of a quad-graph $(x, y, x', y') \in \Diamond_2$.

The Hodge star, which in the continuous theory is defined by $*(f\,dx+g\,dy) = -g\,dx + f\,dy$, is in the discrete case the duality transformation multiplied by the conformal structure:

$$\int_{e^*} *\,\alpha := \rho(e) \int_e \alpha \tag{1}$$

A 1-form $\alpha \in C^1(\Lambda)$ is *of type* $(1,0)$ if and only if, for each quadrilateral $(x, y, x', y') \in \Diamond_2$, $\int_{(y,y')} \alpha = i\,\rho(x, x') \int_{(x,x')} \alpha$, that is to say if $*\alpha = -i\,\alpha$. We define similarly forms of type $(0,1)$ with $+i$ and $-i$ interchanged. A form is *holomorphic*, resp. anti-holomorphic, if it is closed and of type $(1,0)$, resp. of type $(0,1)$. A function $f : \Lambda_0 \to \mathbb{C}$ is holomorphic iff $d_\Lambda f$ is.

We define a wedge product for 1-forms living whether on edges $\Diamond_1$ or on their diagonals Λ_1, as a 2-form living on faces $\Diamond_2$. The formula for the latter is:

$$\iint\limits_{(x,y,x',y')} \alpha \wedge \beta := \frac{1}{2} \left(\int\limits_{(x,x')} \alpha \int\limits_{(y,y')} \beta - \int\limits_{(y,y')} \alpha \int\limits_{(x,x')} \beta \right) \tag{2}$$

The exterior derivative d is a derivation for the wedge product, for functions f, g and a 1-form α:

$$d(fg) = f\,dg + g\,df, \qquad\qquad d(f\alpha) = df \wedge \alpha + f\,d\alpha.$$

Together with the Hodge star, they give rise, in the compact case, to the usual scalar product on 1-forms:

$$(\alpha,\, \beta) := \iint_{\Diamond_2} \alpha \wedge *\bar{\beta} = (*\alpha,\, *\beta) = \overline{(\beta,\, \alpha)} = \tfrac{1}{2} \sum_{e \in \Lambda_1} \rho(e) \int_e \alpha \int_e \bar{\beta} \tag{3}$$

The adjoint $d^* = -*\,d\,*$ of the coboundary d allows to define the discrete Laplacian $\Delta = d^*\,d + d\,d^*$, whose kernel are the harmonic forms and functions. It reads, for a function at a vertex $x \in \Lambda_0$ with neighbours $x' \sim x$:

$$(\Delta f)(x) = \sum_{x' \sim x} \rho(x, x') \left(f(x) - f(x')\right).$$

Hodge theorem: The two $\pm i$-eigenspaces decompose the space of 1-forms, especially the space of harmonic forms, into an orthogonal direct sum. Types are interchanged by conjugation: $\alpha \in C^{(1,0)}(\Lambda) \iff \overline{\alpha} \in C^{(0,1)}(\Lambda)$ therefore

$$(\alpha, \beta) = (\pi_{(1,0)}\alpha, \pi_{(1,0)}\beta) + (\pi_{(0,1)}\alpha, \pi_{(0,1)}\beta)$$

where the projections on $(1,0)$ and $(0,1)$ spaces are

$$\pi_{(1,0)} = \frac{1}{2}(\mathrm{Id} + i*), \qquad \pi_{(0,1)} = \frac{1}{2}(\mathrm{Id} - i*).$$

The harmonic forms of type $(1,0)$ are the *holomorphic* forms, the harmonic forms of type $(0,1)$ are the *anti-holomorphic* forms.

The L^2 norm of the 1-form df, called the Dirichlet energy of the function f, is the average of the usual Dirichlet energies on each independent graph

$$\begin{aligned} E_D(f) := \|df\|^2 = (df,\, df) &= \frac{1}{2} \sum_{(x,x')\in\Lambda_1} \rho(x,x')\, |f(x') - f(x)|^2 \\ &= \frac{E_D(f|_\Gamma) + E_D(f|_{\Gamma^*})}{2}. \end{aligned} \tag{4}$$

The conformal energy of a map measures its conformality defect, relating these two harmonic functions. A conformal map fulfills the Cauchy-Riemann equation

$$*\, df = -i\, df. \tag{5}$$

Therefore a quadratic energy whose null functions are the holomorphic ones is

$$E_C(f) := \tfrac{1}{2}\|df - i * df\|^2. \tag{6}$$

It is related to the Dirichlet energy through the same formula as in the continuous:

$$\begin{aligned} E_C(f) &= \tfrac{1}{2}\,(df - i * df,\, df - i * df) \\ &= \tfrac{1}{2}\|df\|^2 + \tfrac{1}{2}\|{-i} * df\|^2 + \mathrm{Re}(df,\, -i * df) \\ &= \|df\|^2 + \mathrm{Im} \iint_{\diamondsuit_2} df \wedge \overline{df} \\ &= E_D(f) - 2\mathcal{A}(f) \end{aligned} \tag{7}$$

where the area of the image of the application f in the complex plane has the same formulae (the second one meaningful on a simply connected domain)

$$\mathcal{A}(f) = \frac{i}{2} \iint_{\diamondsuit_2} df \wedge \overline{df} = \frac{i}{4} \oint_{\partial\diamondsuit_2} f\, \overline{df} - \overline{f}\, df \tag{8}$$

as in the continuous case. For a face $(x, y, x', y') \in \diamondsuit_2$, the algebraic area of the oriented quadrilateral $\Big(f(x), f(x'), f(y), f(y')\Big)$ is given by

$$\begin{aligned} \iint_{(x,y,x',y')} df \wedge \overline{df} &= i\, \mathrm{Im} \Big((f(x') - f(x)) \overline{(f(y') - f(y))} \Big) \\ &= -2i\mathcal{A}\Big(f(x), f(x'), f(y), f(y')\Big). \end{aligned}$$

When a holomorphic reference map $z : \Lambda_0 \to \mathbb{C}$ is chosen, an holomorphic (resp. anti-holomorphic) 1-form df is, locally on each pair of dual diagonals, proportional to dz, resp. $d\bar{z}$, so that the decomposition of the exterior derivative into holomorphic and anti-holomorphic parts yields $df \wedge \overline{df} = \big(|\partial f|^2 + |\bar{\partial} f|^2\big)\, dz \wedge d\bar{z}$ where the derivatives naturally live on faces.

3 Algorithm

The theory described above is straightforward to implement. The most sensitive part is based on a minimizer procedure which finds the minimum of the Dirichlet energy for a discrete Riemann surface, given some boundary conditions. Here is the crude algorithm that we are going to detail.

Basis of holomorphic forms(a discrete Riemann surface S)
find a normalized homotopy basis $\aleph$ of $\diamondsuit(S)$
for all $\aleph_k$ **do**
  compute $\aleph_k^\Gamma$ and $\aleph_k^{\Gamma^*}$
  compute the real discrete harmonic form ω_k on Γ s.t. $\oint_\gamma \omega_k = \gamma \cdot \aleph_k^\Gamma$
  (check ω_k is harmonic on Γ)
  compute the form $*\omega_k$ on Γ^*
  (check $*\omega_k$ is harmonic on Γ^*)
  compute its holonomies $(\oint_{\aleph_\ell^{\Gamma^*}} *\omega_k)_{k,\ell}$ on Γ^*
  do likewise for ω_k^* on Γ^*
end for
do some linear algebra (R is a rectangular complex matrix) to get the basis of holomorphic forms $(\zeta_k)_k = R(\mathrm{Id} + i\,*)(\omega_k)_k$ s.t. $(\oint_{\aleph_\ell^\Gamma} \zeta_k) = \delta_{k,\ell}$
define the period matrix $\Pi_{k,\ell} := (\oint_{\aleph_\ell^{\Gamma^*}} \zeta_k)$
do likewise for $(\zeta_k^*)_k$ and $\Pi_{k,\ell}^* := (\oint_{\aleph_\ell^\Gamma} \zeta_k^*)$

Finding a normalized homotopy basis of a connected cellular decomposition is performed by several well known algorithms. The way we did it is to select a root vertex and grow from there a spanning tree, by computing the vertices at combinatorial distance d from the root and linking each one of them to a unique vertex at distance $d-1$, already in the tree. Repeat until no vertices are left.

Then we inflate this tree into a polygonal fundamental domain by adding faces one by one to the domain, keeping it simply connected: We recursively add all the faces which have only one edge not in the domain. We stop when all the remaining faces have at least two edges not in the domain.

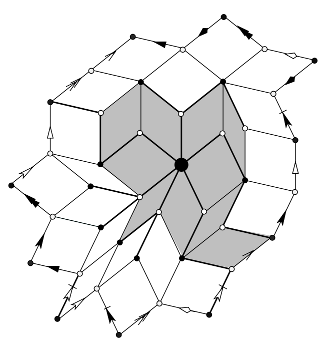

Then we pick one edge (one of the closest to the root) as defining the first element of our homotopy basis: adding this edge to the fundamental domain yields a non simply connected cellular decomposition and the spanning tree gives us a rooted cycle of this homotopy type going down the tree to the root. It is (one of) the combinatorially shortest in its (rooted) homology class. We add faces recursively in a similar way until we can no go further, we then choose a new homotopy basis element, and so on until every face is closed. At the end we have a homotopy basis. We compute later on the intersection numbers in order to normalize it.

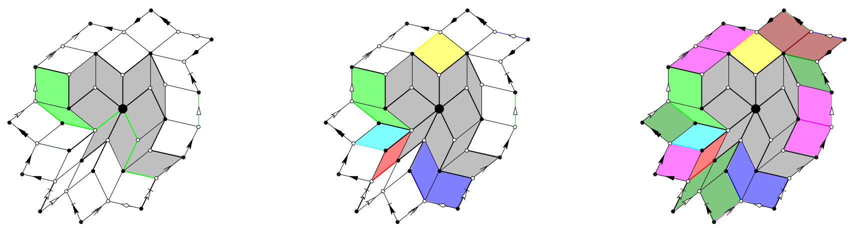

We compute the unique real harmonic form η associated with each cycle $\aleph$ such that $\oint_\gamma \eta = \gamma \cdot \aleph$. This is done by a minimizing procedure which finds the unique harmonic function f on the graph Γ, split along $\aleph$, whose vertices are duplicated, which is zero at the root and increases by one when going across $\aleph$. This is done by linking the values at the duplicated vertices, in effect yielding a harmonic function on the universal cover of Γ. The harmonic 1-form $d\,f$ doesn't depend on the chosen root nor on the representative $\aleph$ in its homology class.

4 Numerics

We begun with testing discrete surfaces of known moduli in order to investigate the quality of the numerics and the robustness of the method. We purposely chose to stick with raw *double* 15-digits numbers and a linear algebra library which is fast but not particularly accurate. In order to be able to compare period matrices, we used a Siegel reduction algorithm [10] to map them by a modular transformation to the same fundamental domain.

4.1 Surfaces tiled by squares

Robert Silhol supplied us with sets of surfaces tiled by squares for which the period matrix are known [24, 7, 23, 6, 22]. There are translation and half-translation surfaces: In these surfaces, each horizontal side is glued to a horizontal side, a vertical to a vertical, and the identification between edges of the fundamental polygon are translations for translation surfaces and translations followed by a half-twist for half-translations. The discrete conformal structure for these surfaces is very simple: the combinatorics is given by the gluing conditions and the conformal parameter $\rho \equiv 1$ is constant.

The genus one examples are not interesting because this 1-form is then the unique holomorphic form and there is nothing to compute (the algorithm does give back this known result). Genus 2 examples are non trivial because a second holomorphic form has to be computed.

The translation surfaces are particularly adapted because the discrete 1-form read off the picture is already a discrete holomorphic form. Therefore the computations are accurate even for a small number of squares. Finer squares only blur the result with numerical noise. For half-translation surfaces it is not the case, a continuous limit has to be taken in order to get a better approximation.

Surface & Period Matrix	Numerical Analysis	
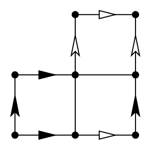 $\Omega_1 = \frac{i}{3}\begin{pmatrix} 5 & -4 \\ -4 & 5 \end{pmatrix}$	#vertices	$\lVert\Omega_D - \Omega_1\rVert_\infty$
	25	$1.13 \cdot 10^{-8}$
	106	$3.38 \cdot 10^{-8}$
	430	$4.75 \cdot 10^{-8}$
	1726	$1.42 \cdot 10^{-7}$
	6928	$1.35 \cdot 10^{-6}$
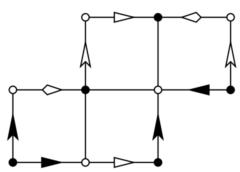 $\Omega_2 = \frac{1}{3}\begin{pmatrix} -2+\sqrt{8}i & 1-\sqrt{2}i \\ 1-\sqrt{2}i & -2+\sqrt{8}i \end{pmatrix}$	#vertices	$\lVert\Omega_D - \Omega_2\rVert_\infty$
	14	$3.40 \cdot 10^{-2}$
	62	$9.51 \cdot 10^{-3}$
	254	$2.44 \cdot 10^{-3}$
	1022	$6.12 \cdot 10^{-4}$
	4096	$1.53 \cdot 10^{-4}$
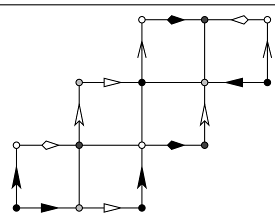 $\Omega_3 = \frac{i}{\sqrt{3}}\begin{pmatrix} 2 & -1 \\ -1 & 2 \end{pmatrix}$	#vertices	$\lVert\Omega_D - \Omega_3\rVert_\infty$
	22	$3.40 \cdot 10^{-3}$
	94	$9.51 \cdot 10^{-3}$
	382	$2.44 \cdot 10^{-4}$
	1534	$6.12 \cdot 10^{-5}$
	6142	$1.53 \cdot 10^{-6}$

Using 15 digits numbers, the theoretical numerical accuracy is limited to 8 digits because our energy is quadratic therefore half of the digits are lost. Using an arbitrary precision toolbox or Cholesky decomposition in order to solve the linear system would allow for better results but it is not the point here.

4.2 Wente torus

For a first test of the numerics on a an immersed surface in $\mathbb{R}^3$ our choice is the famous CMC-torus discovered by Wente [27] for which an explicit immersion formula exists in terms of theta functions [3]. The modulus of the rhombic Wente torus can be read from the immersion formula:

$$\tau_w \approx 0.41300\ldots + 0.91073\ldots i \approx \exp(i1.145045\ldots.).$$

We compute several regular discretization of the Wente torus (Fig. 1) and generate discrete conformal structures using ρ_{ex} that are imposed by the extrinsic Euclidean metric of $\mathbb{R}^3$ as well as ρ_{in} which are given by the intrinsic

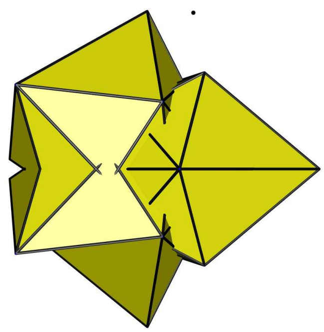

Grid : 10×10

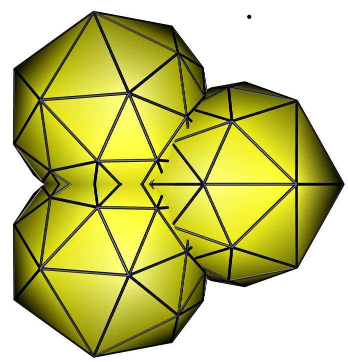

Grid : 20×20

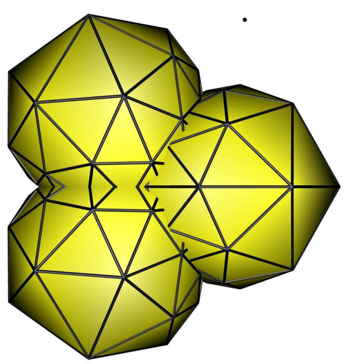

Grid : 40×40

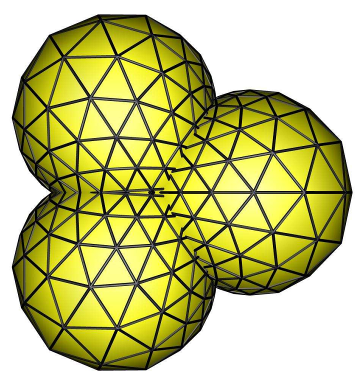

Grid : 80×80

Figure 1: Regular Delaunay triangulations of the Wente torus

flat metric of the surface. For a sequence of finer discretizations of a smooth immersion, the two sets of numbers come closer and closer. For these discrete conformal structures we compute again the moduli which we denote by τ_{ex} and τ_{im} and compare them with τ_w from above:

Grid	$\|\tau_{\text{in}} - \tau_w\|$	$\|\tau_{\text{ex}} - \tau_w\|$
10×10	$5.69 \cdot 10^{-3}$	$5.00 \cdot 10^{-3}$
20×20	$2.00 \cdot 10^{-3}$	$5.93 \cdot 10^{-3}$
40×40	$5.11 \cdot 10^{-4}$	$1.85 \cdot 10^{-3}$
80×80	$2.41 \cdot 10^{-4}$	$6.00 \cdot 10^{-4}$

For the lowest resolution the accuracy of τ_{ex} is slightly better then the one of τ_{in}. For all other the discrete conformal structures with the intrinsically generated ρ_{in} yields significant higher accuracy.

4.3 Lawson surface

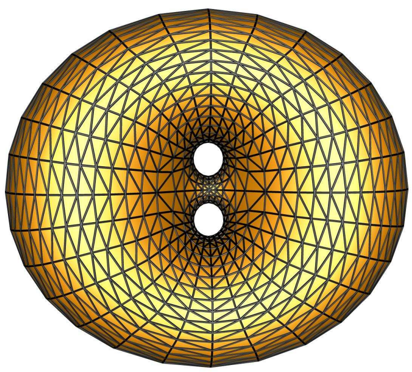

1162 vertices

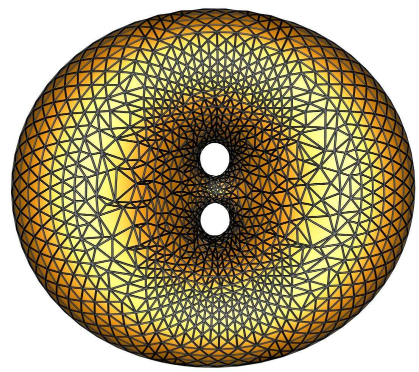

2498 vertices

Figure 2: Delaunay triangulations of the Lawson surface

Finally we apply our method to compute the period matrix of Lawson's famous genus 2 Willmore surface [15]. Konrad Polthier [21] supplied us with several resolution of the surface which are generated by a coarsening and mesh beautifying process of a very fine approximation of the Lawson surface (Fig. 2). Our numerical analysis gives evidence that the period matrix of the Lawson surface is

$$\Omega_l = \frac{i}{\sqrt{3}} \begin{pmatrix} 2 & -1 \\ -1 & 2 \end{pmatrix}$$

which equals the period matrix Ω_3 of the third example from Sec. 4.1. Once conjectured that these two surfaces are conformally equivalent, it is a matter of checking that the symmetry group of the Lawson genus two surface yields indeed this period matrix, which was done, without prior connection, in [1]. An explicit conformal mapping of the surfaces can be found manually: The genus 2 Lawson surface exhibits by construction four points with an order six symmetry and six points of order four, which decomposes the surface into 24 conformally equivalent triangles, of angles $\frac{\pi}{6}$, $\frac{\pi}{2}$, $\frac{\pi}{2}$. Therefore an algebraic equation for the Lawson surface is $y^2 = x^6 - 1$, with six branch points at the roots of unity. The correspondance between the points in the square picture of the surface and the double sheeted cover of the complex plane is done in Fig. 3. In particular the center of the six squares are sent to the branch points, the vertices are sent to the two copies of 0 (black and dark gray) and ∞ (white and light gray), the square are sent to double sheeted two gons corresponding to a sextant.

Similarly to Sec. 4.2 we compute the period matrices Ω_{ex} and Ω_{in} for different resolutions utilizing weights imposed by the extrinsic and intrinsic metric and compare the results with our conjectured period matrix for the Lawson surface Ω_l:

#vertices	$\|\Omega_{\text{in}} - \Omega_l\|_\infty$	$\|\Omega_{\text{ex}} - \Omega_l\|_\infty$
1162	$1.68 \cdot 10^{-3}$	$1.68 \cdot 10^{-3}$
2498	$3.01 \cdot 10^{-3}$	$3.20 \cdot 10^{-3}$
10090	$8.55 \cdot 10^{-3}$	$8.56 \cdot 10^{-3}$

Our first observation is that the matrices Ω_{ex} and Ω_{in} almost coincide. Hence the method for computing the ρ seems to have only little influence on this result (compare also Sec. 4.2). Further we see that figures of the higher resolution surface, i.e. with 2498 and 10090 vertices ar worse than the coarsest one with 1162 vertices. The mesh beautifying process was most successful on the coarsest triangulation of the Lawson surface (Fig. 2). The quality of the mesh has a significant impact on the accuracy of our computation: One can see that the triangles on the coarsest example are of even shapes with comparable side lengths, while the finer resolution contains thin triangles with small angles. The convergence speed proven in [18] is governed by this smallest angles, accounting for the poor result.

References

[1] M. V. Babich, A. I. Bobenko, and V. B. Matveev. Solution of nonlinear equations, integrable by the inverse problem method, in Jacobi theta-functions and the symmetry of algebraic curves. *Izv. Akad. Nauk SSSR Ser. Mat.*, 49(3):511–529, 672, 1985.

[2] M. Ben-Chen, C. Gotsman, and G. Bunin. Conformal flattening by curvature prescription and metric scaling. In *Computer Graphics Forum*, 27(2). Proc. Eurographics, 2008. PDF.

[3] A. I. Bobenko. All constant mean curvature tori in $\mathbf{R}^3$, S^3, H^3 in terms of theta-functions. *Math. Ann.*, 290(2):209–245, 1991.

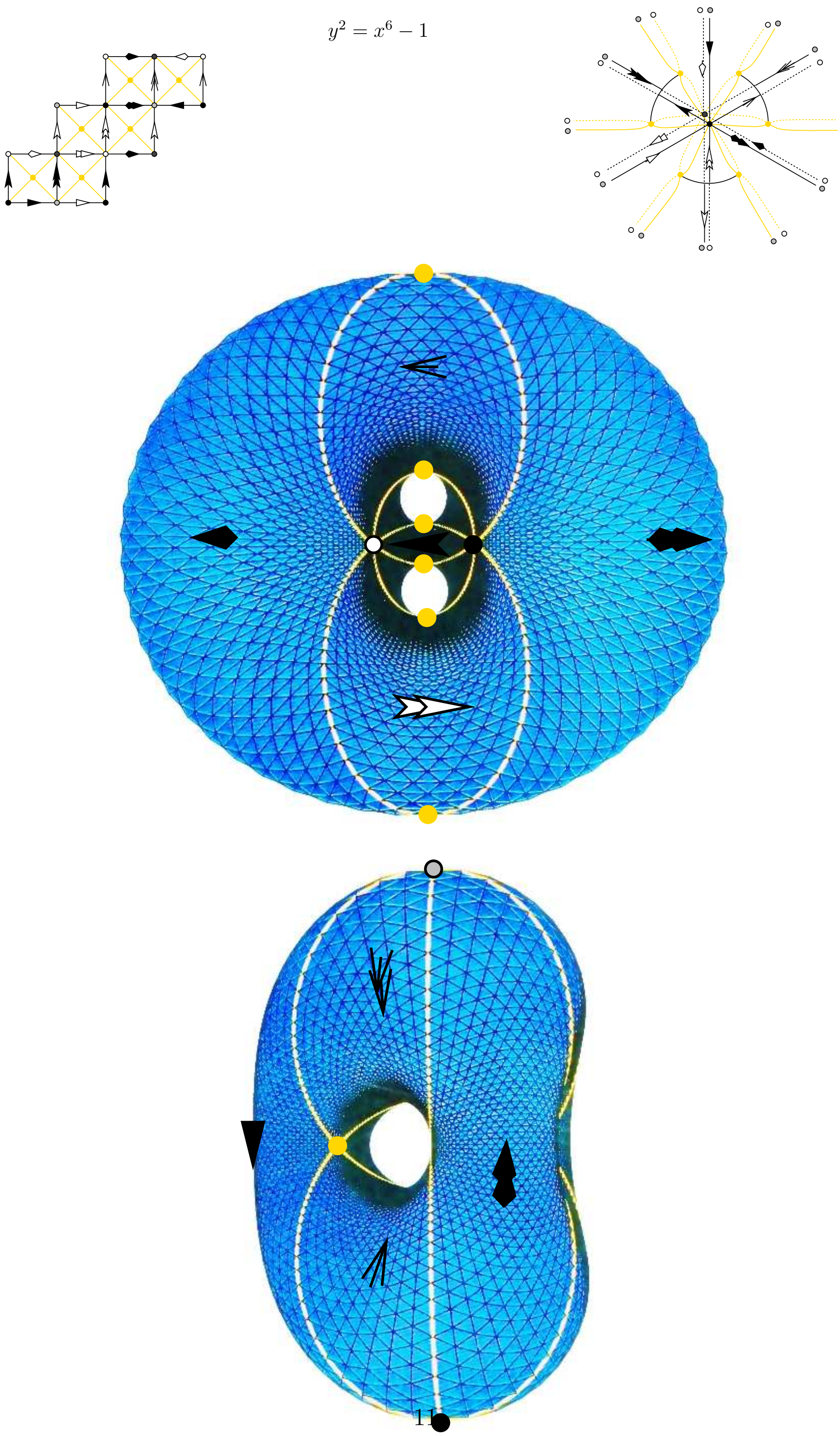

Figure 3: The Lawson surface is conformally equivalent to a surface made of squares.

[4] A. I. Bobenko, C. Mercat, and Y. B. Suris. Linear and nonlinear theories of discrete analytic functions. Integrable structure and isomonodromic Green's function. *J. Reine Angew. Math.*, 583:117–161, 2005. `math.DG/0402097`.

[5] A. I. Bobenko and B. A. Springborn. A discrete laplace-beltrami operator for simplicial surfaces. *Discrete and Computational Geometry*, 38:4:740–756, 2007. `math.DG/0503219`.

[6] P. Buser and R. Silhol. Geodesics, periods, and equations of real hyperelliptic curves. *Duke Math. J.*, 108(2):211–250, 2001.

[7] P. Buser and R. Silhol. Some remarks on the uniformizing function in genus 2. *Geom. Dedicata*, 115:121–133, 2005.

[8] R. Costa-Santos and B. M. McCoy. Dimers and the critical Ising model on lattices of genus > 1. *Nuclear Phys. B*, 623(3):439–473, 2002. `hep-th/0109167`.

[9] R. Costa-Santos and B. M. McCoy. Finite size corrections for the Ising model on higher genus triangular lattices. *J. Statist. Phys.*, 112(5-6):889–920, 2003.

[10] B. Deconinck, M. Heil, A. Bobenko, M. van Hoeij, and M. Schmies. Computing Riemann theta functions. *Math. Comp.*, 73(247):1417–1442, 2004. ams.

[11] M. Desbrun, E. Kanso, and Y. Tong. Discrete differential forms for computational modeling. In A. I. Bobenko, P. Schröder, J. M. Sullivan, and G. M. Ziegler, editors, *Discrete Differential Geometry*, volume 38 of *Oberwolfach Seminars*, pages 287–323. Birkhaüser, 2008.

[12] M. Desbrun, M. Meyer, and P. Alliez. Intrinsic parameterizations of surface meshes. In *Computer Graphics Forum*, 21, pages 209–218. Proc. Eurographics, 2002. `citeseer`.

[13] R. J. Duffin. Potential theory on a rhombic lattice. *J. Combinatorial Theory*, 5:258–272, 1968.

[14] J. Ferrand. Fonctions préharmoniques et fonctions préholomorphes. *Bull. Sci. Math. (2)*, 68:152–180, 1944.

[15] J. H.B. Lawson. Complete minimal surfaces in S^3. *Ann. of Math.*, 92:335–374, 1970.

[16] M. Jin, Y. Wang, S.-T. Yau, and X. Gu. Optimal global conformal surface parameterization. In *VIS '04: Proceedings of the conference on Visualization '04*, 2004.

[17] L. Kharevych, B. Springborn, and P. Schröder. Discrete conformal mappings via circle patterns. *ACM Trans. Graph.*, 25(2):412–438, 2006. citeseer.

[18] C. Mercat. Discrete Riemann surfaces and the Ising model. *Comm. Math. Phys.*, 218(1):177–216, 2001.

[19] C. Mercat. Exponentials form a basis of discrete holomorphic functions on a compact. *Bull. Soc. Math. France*, 132(2):305–326, 2004. math-ph/0210016.

[20] C. Mercat. Discrete Riemann surfaces. In A. Papadopoulos, editor, *Handbook of Teichmüller Theory, vol. I*, volume 11 of *IRMA Lect. Math. Theor. Phys.*, pages 541–575. Eur. Math. Soc., Zürich, 2007. arXiv:0802.1612.

[21] U. Pinkall and K. Polthier. Computing discrete minimal surfaces and their conjugates. *Experiment. Math.*, 2(1):15–36, 1993. citeseer.

[22] R. E. Rodríguez and V. González-Aguilera. Fermat's quartic curve, Klein's curve and the tetrahedron. In *Extremal Riemann surfaces (San Francisco, CA, 1995)*, volume 201 of *Contemp. Math.*, pages 43–62. Amer. Math. Soc., Providence, RI, 1997.

[23] R. Silhol. Period matrices and the Schottky problem. In *Topics on Riemann surfaces and Fuchsian groups (Madrid, 1998)*, volume 287 of *London Math. Soc. Lecture Note Ser.*, pages 155–163. Cambridge Univ. Press, Cambridge, 2001.

[24] R. Silhol. Genus 2 translation surfaces with an order 4 automorphism. In *The geometry of Riemann surfaces and abelian varieties*, volume 397 of *Contemp. Math.*, pages 207–213. Amer. Math. Soc., Providence, RI, 2006.

[25] Y. Tong, P. Alliez, D. Cohen-Steiner, and M. Desbrun. Designing Quadrangulations with Discrete Harmonic Forms. In A. Sheffer and K. Polthier, editors, *Symposium on Geometry Processing*, pages 201–210, Cagliari, Sardinia, Italy, 2006. Eurographics Association. acm.

[26] M. Wardetzky. *Discrete Differential Operators on Polyhedral Surfaces - Convergence and Approximation.* PhD thesis, FU Berlin, 2006.

[27] H. C. Wente. Counterexample to a conjecture of H. Hopf. *Pacific J. Math.*, 121(1):193–243, 1986.